

The photoisomerization of aqueous ICN studied by subpicosecond transient absorption spectroscopy

Jane Larsen, Dorte Madsen, Jens-Aage Poulsen, Tina D. Poulsen, Søren R. Keiding, and Jan Thøgersen

Citation: *The Journal of Chemical Physics* **116**, 7997 (2002); doi: 10.1063/1.1467897

View online: <http://dx.doi.org/10.1063/1.1467897>

View Table of Contents: <http://scitation.aip.org/content/aip/journal/jcp/116/18?ver=pdfcov>

Published by the [AIP Publishing](#)

Articles you may be interested in

Ionization and dissociation dynamics of vinyl bromide probed by femtosecond extreme ultraviolet transient absorption spectroscopy

J. Chem. Phys. **140**, 064311 (2014); 10.1063/1.4865128

The dissociation dynamics of HeI 35 Cl ($B, v' = 2, 3$) complexes with varying amounts of internal energy

J. Chem. Phys. **122**, 044318 (2005); 10.1063/1.1829971

Photodissociation of ICN at the liquid/vapor interface of water

J. Chem. Phys. **121**, 2253 (2004); 10.1063/1.1765093

Molecular dynamics study of the photodissociation and photoisomerization of ICN in water

J. Chem. Phys. **119**, 2127 (2003); 10.1063/1.1585019

Hybrid quantum/classical study of ICN in an Ar matrix: Photofragmentation and cage exit

J. Chem. Phys. **113**, 1027 (2000); 10.1063/1.481882



The photoisomerization of aqueous ICN studied by subpicosecond transient absorption spectroscopy

Jane Larsen, Dorte Madsen, Jens-Aage Poulsen, Tina D. Poulsen, Søren R. Keiding,^{a)} and Jan Thøgersen

Department of Chemistry, Aarhus University, Langelandsgade 140, DK 8000 Århus C, Denmark

(Received 20 December 2001; accepted 13 February 2002)

The photolysis of aqueous ICN is studied by transient absorption spectroscopy covering the spectral range from 227 to 714 nm with 0.5 ps time resolution. The experimental data show that when ICN(aq) is photolyzed at 266 nm, it dissociates into I and CN and both the $I(^2P_{3/2})$ and $I(^2P_{1/2})$ channels are populated. Approximately half the fragments escape the solvent cage while the remainder recombines within the solvent cage during the first picosecond. The majority of the recombinations form ICN while only a minor fraction produces the metastable INC isomer. INC and ICN relax to the vibrational ground state within 1 ps in good agreement with theoretical estimates based on the golden rule formalism as well as molecular dynamics simulations. Diffusive recombination involving fragments that have escaped the solvent cage further reduces the quantum yield of I and CN to 10% during the following 100 ps. This recombination produces exclusively ICN. © 2002 American Institute of Physics. [DOI: 10.1063/1.1467897]

I. INTRODUCTION

One of the most prominent features of liquid-phase reaction dynamics is the solvents ability to inhibit reactions by caging the products. This phenomenon is readily observed in many photodissociation processes where a substantial fraction of the photoproducts is kept within the confines of the first solvent shell and forced to recombine in a cage back reaction. Triatomic molecules are the smallest species that may recombine in a configuration different from that of the parent molecule, while still being sufficiently simple to allow for a detailed calculation of the solvent induced recombination process. In the triatomic systems where geminate recombination has been studied in detail, fast geminate recombination to the parent molecule on the electronic ground state is by far the dominating recombination channel within the solvent cage.¹⁻⁶ These studies indicate that upon excitation to the dissociative potential energy surface the molecule never really dissociates but rather performs a few oscillations around a highly distorted geometry dictated by the excited state potential and the solvent barrier before it nonadiabatically transfers to the ground state.

The photodissociation and subsequent recombination of solvated iodine cyanide may progress differently: Gas-phase iodine cyanide has two bound geometries with a calculated 1.23 eV difference between the binding energy of ground state ICN [$D_0(\text{I-CN}) = 3.17$ eV]⁷ and its metastable isomer, INC.⁸ A barrier of 0.8 eV separates the two geometries and while both molecules are linear their interconversion transition state is virtually an isosceles triangle.⁸ The lowest excited states of ICN, accessible from the ICN($X^1\Sigma^+$) ground state, are $^3\Pi_1$, $^3\Pi_{0+}$, and $^1\Pi_1$. When excited to these states with $h\nu \sim 5$ eV, gas-phase ICN dissociates into nearly equal amounts of $I(^2P_{3/2}) + \text{CN}(^2\Sigma^+)$, and $I(^2P_{1/2}) + \text{CN}(^2\Sigma^+)$ as

indicated in Fig. 1.⁹ The $^3\Pi_1$ and $^1\Pi_1$ states correlate with ground state $I(^2P_{3/2})$, while $^3\Pi_{0+}$ correlates with the excited $I(^2P_{1/2})$ channel. A considerable fraction of the excess energy liberated by the photodissociation of ICN(g) is transferred to the CN fragment as rotational energy, whereas the CN fragment is left vibrationally cold.⁹ Detailed molecular dynamics (MD) simulations of the photolysis of ICN in liquid chloroform performed by Benjamin show that the high angular momentum enables the CN fragment to rotate rapidly, thus facilitating the formation of INC within the solvent cage.¹⁰ More specifically: If the ICN molecule is excited to the $^3\Pi_1$ state, the MD simulations predict a 75% recombination yield on the electronic ground state after 1 ps. The recombination of I and CN produces ICN and INC. ICN and INC are formed vibrationally excited and the simulations predict several interconversions between the two isomers during the first couple of picoseconds resulting in a relative yield of 73% ICN and 27% INC. Of the remaining ICN molecules excited to the $^3\Pi_1$ state, 2/3 escape the cage in 0.5 ps while 1/3 stay excited as ICN* or INC* for more than 5 ps. If, on the other hand, the ICN molecule is excited to the $^3\Pi_{0+}$ state, 85% of the molecules recombine on the excited $^3\Pi_{0+}$ state with a 7:3 ratio between the yield of ICN* and INC*, while the rest escape the cage within the first picosecond. Nonadiabatic transitions from $^3\Pi_{0+}$ to the $^3\Pi_1$ and $^1\Pi_1$ states are not considered by the simulations, but are expected to lead to a behavior similar to that observed for dissociation on the $^3\Pi_1$ state. Photodissociation following excitation of the $^1\Pi_1$ state is not included in the MD simulations and for reasons described in Sec. II excitation to this state turns out not to be important to the present work.

The high isomerization yield predicted by the MD simulations and the possibility of observing the formation of both ICN and INC make ICN a promising candidate for studying the details of geminate recombination processes in liquids

^{a)}Electronic mail: Keiding@chem.au.dk

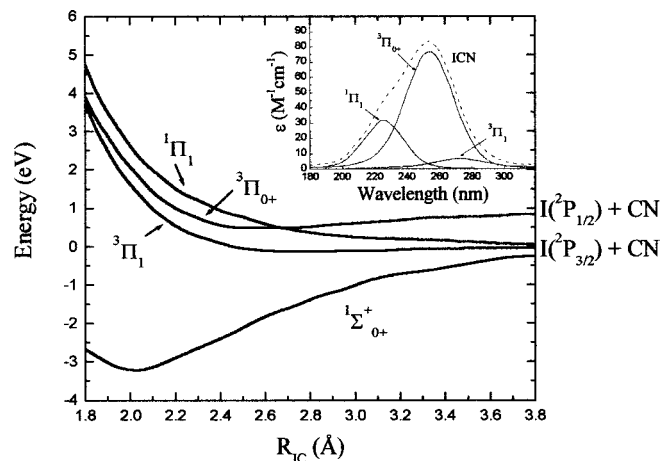


FIG. 1. Potential energy surface (Ref. 34) and absorption spectrum (insert)—Ref. 15—of gas-phase ICN. Photodissociation of ICN results in production of $I(^2P_{3/2}) + CN(^2\Sigma^+)$ and $I(^2P_{1/2}) + CN(^2\Sigma^+)$. Only the $I(^2P_{3/2}) + CN(^2\Sigma^+)$ channel correlates with the ICN ground state.

and solid rare-gas matrices.^{10–14} Experimentally, liquid phase photodynamics of ICN has so far only been addressed by Wan *et al.*, who studied the photolysis of ICN in chloroform by monitoring the transient absorption of the CN molecule.¹² These measurements showed an instrument limited (<300 fs) formation of CN followed by ~2–4 ps decay ascribed to recombination of CN with I within the solvent cage and a 76 ps decay ascribed to H or Cl abstraction from the solvent. However, the strong UV absorption of chloroform precluded the observation of the iodine fragments as well as the recombination products, and the process of photoisomerization of ICN within the solvent cage has therefore yet to be observed experimentally.

In this work we present direct experimental evidence for subpicosecond photoisomerization of aqueous ICN followed by efficient energy dissipation to the solvent, which cools the isomer to its lowest vibrational levels in ≈ 1 ps. Second, our measurements show that while a substantial part of the ICN reformation occurs by diffusion 5–10 ps after the photodissociation, the INC molecules are exclusively produced by geminate recombination inside the first solvation shell. The lack of INC formation by diffusive recombination is ascribed to steric hindrance by water molecules hydrogen bonding to the nitrogen atom of the solvated CN radical. The photolysis of aqueous ICN thus presents a striking example of how solvents may both assist and inhibit chemical reactions.

II. STATIC ABSORPTION SPECTRA

The experimental technique of transient absorption spectroscopy identifies the species involved in the photolysis by their absorption spectra. Hence, this section presents the steady state absorption spectra of ICN, INC, I, and CN. The static absorption spectra of aqueous ICN recorded by a Uvikon 860 (Kontron Instruments) spectrophotometer with a spectral resolution of 2 nm is shown in Fig. 2. The spectrum peaks at 222 nm with a maximum extinction coefficient of $181 \pm 5 \text{ M}^{-1} \text{ cm}^{-1}$ and has a width of 50 nm [full width at half maximum (FWHM)]. The ICN(aq) absorption maxi-

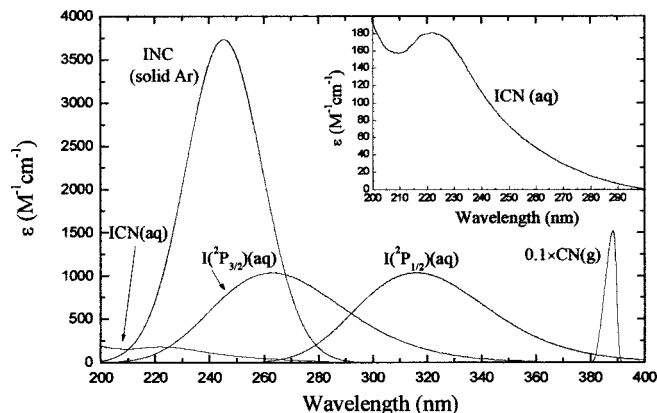


FIG. 2. The static absorption spectra of INC(Ar matrix)—Ref. 11, CN(g)—Refs. 7 and 35, and $I(^2P_{3/2})(aq)$ —Ref. 18 and ICN. The absorption spectrum of aqueous ICN was measured in this work. The absorption spectrum of $I(^2P_{1/2})$ was estimated from the $I(^2P_{3/2})$ absorption spectrum utilizing the approach described in Refs. 20 and 17.

um is thus blueshifted by 28 nm and the extinction coefficient is nearly twice of that reported for gas-phase ICN.^{9,15,16} The $X^1\Sigma^+ \rightarrow 1^1\Pi_1$ transition responsible for the short wavelength part of the ICN(g) absorption spectrum has little intensity at the 266 nm photolysis wavelength used in the present measurements (see Fig. 1). Hence, assuming the blueshift of ICN(aq) arises from a common spectral shift of all three transitions this paper mainly studies the photodynamics following excitation to the $3^1\Pi_1$ and $3^1\Pi_0$ states.

The absorption spectrum of aqueous $I(^2P_{3/2})$, shown in Fig. 2, results from a charge transfer complex between ground state $I(^2P_{3/2})$ and water.^{17–19} The absorption spectrum of the $I(^2P_{1/2}):H_2O$ has, to the best of our knowledge, not been determined experimentally, nor have we found any reports on its extinction coefficient. Instead, the spectral shift relative to that of the ground state complex may, to a first approximation, be calculated using a semiempirical approach,^{17,20} which essentially shift the absorption band by the fine-structure splitting. The $I(^2P_{1/2}):H_2O$ spectrum presented in Fig. 2 is that of the $I(^2P_{3/2}):H_2O$ complex redshifted to 314 nm, while keeping the extinction coefficient of the ground state complex.

Likewise, INC has never been observed in liquid solution and the only absorption spectra available are those measured in solid argon and krypton matrices.¹¹ The extinction coefficient of INC in Argon presented in Fig. 2 has been derived from the spectrum of INC calibrated with the known ICN extinction coefficient using the relative yield of ICN and INC from the steady state photolysis of ICN in argon matrices.^{8,11} However, just as the extinction coefficient of aqueous ICN is almost twice the value measured in gas phase, the extinction coefficient of aqueous INC may differ from that in solid noble gases, and if so, the quantum yields reported in the present work will change accordingly.

The gas-phase CN radical is known to have a very strong absorption at 388 nm pertaining to the $X \rightarrow B$ transition (see Fig. 2) and measurements reported by Wan *et al.*¹² also indicate a strong blue absorption in chloroform. Studies of the spectral shift of the CN radical in noble gas matrices show

significant redshifts increasing to as much as 1000 cm^{-1} in CN–Xe complexes.²¹ The absorption spectrum of CN in water, on the other hand, has not been determined experimentally and is likely to be perturbed by the highly polar environment. In order to estimate the spectral shift caused by hydration we have calculated the excitation energy of the CN:H₂O complex. First the X→B excitation energy of gas-phase CN was calculated using multiconfigurational self-consistent field theory with a correlation consistent one-electron basis set augmented with one set of diffuse functions with triple zeta quality (/aug-cc-pVTZ). The resulting gas-phase excitation energy of $E(\text{CN})_{\text{theory}}=3.31\text{ eV}$ is in good agreement with the experimental value of $E(\text{CN})_{\text{exp}}=3.20\text{ eV}$. Having tested the calculations on gas-phase CN the excitation energy of the CN:H₂O complex was then calculated for a collinear geometry with the OH bond aligned along the CN bond and for the two separate cases of H facing C and N, respectively. The intermolecular distance between H and C (and H and N) was varied from 3.36 to 3.9 Å. The resulting excitation energy of the X→B transition was redshifted by 0.02–0.7 eV (377–475 nm) depending on the position of the CN radical relative to the water molecule. In addition to the pronounced spectral shift, the high sensitivity to the solvent geometry suggests a strong broadening of the CN(aq) absorption spectrum relative to that of CN(g).

Although lacking spectroscopic properties of the reactants necessitate several assumptions and calculations, the experimental data to be presented give evidence for a consistent picture of the molecular dynamics as well as the static absorption spectra.

III. EXPERIMENTAL SETUP

The transient absorption spectrometer used in this work is identical to the one described by Thomsen *et al.*²² and is only described briefly: 800 nm pulses emitted by an amplified titanium:sapphire laser were frequency tripled to generate the 266 nm pump pulses utilized for photolyzing ICN. The pump beam was sent through a variable delay line and a $\lambda/2$ wave plate, before it was focused behind the sample cell by an $f=50\text{ cm}$ CaF₂ lens. The profile of the pump beam at the sample cell was measured by means of a scanning pinhole and the semiaxes of the elliptical beam crosssection were $0.16\text{ mm}\pm 0.01\text{ mm}$ and $0.11\text{ mm}\pm 0.01\text{ mm}$ (half width at half maximum). The pump pulse energy was kept at $55\text{ }\mu\text{J}$ in order to reduce contributions to the measured absorption transients from hydrated electrons and OH and H radicals produced by two-photon dissociation of water.²² The probe pulses were generated by a combination of supercontinuum generation, second harmonic generation, and sum-frequency mixing. A beamsplitter divided the probe beam into a signal and a reference beam, which were measured by two matched photodiodes and boxcar integrators. The pump beam was modulated at 0.5 kHz, locked to the 1 kHz repetition rate of the laser amplifier, and made to cross the signal beam inside the sample cell at an angle of $\approx 5^\circ$. A $\lambda/2$ wave plate in the pump beam was adjusted so as to keep the polarization of the pump beam perpendicular to that of the probe beam.

Iodine cyanide was prepared by dissolving 27 g (0.55 mol) of sodium cyanide in 100 ml, three times distilled water at 0°C. A total of 127 g of iodine (0.50 mol) was added in small portions while stirring the solution at 0°C. Subsequently, 120 ml of diethyl ether was added and the solution was stirred for 15 min. The aqueous layer was separated from the ether layer in a precooled separatory funnel and extracted six times with cold diethyl ether. The ether was left standing at room temperature for 1 h in a beaker with a large surface area allowing most of the ether to evaporate. The resulting white, needle-shaped crystals were separated from the residual ether by suction filtration and washed five times with cold water. The crystalline iodine cyanide was air dried for 30 min yielding a total of 30–40 g (50%–60%) iodine cyanide.

Immediately before use, 8.5 g of iodine cyanide was dissolved in 0.5 l of three times distilled water, yielding a concentration of $c=0.11\text{ M}$ corresponding to an optical density of $\text{OD}=0.7$ at 266 nm in the 1.8-mm-thick flow cell. The flow rate was adjusted to ensure a fresh sample of ICN for each laser pulse. The reproducibility of the transient absorption data was tested among consecutive scans as well as by repeating the experiments on different days using different samples. No measurable degradation of the ICN solution was observed during a measurement, but the slow buildup of permanent photoproducts necessitated frequent replacement of the ICN solution. From numerous measurements we found that the data could be measured on a common scale with an uncertainty of $\pm 10\%$.

IV. EXPERIMENTAL RESULTS

A. Assignment of the absorption transients

The photoinduced absorption, $\Delta A(\lambda, t)$, of aqueous ICN produced by the 266 nm pump pulse and measured at 500 cm^{-1} intervals in the spectral range from 227 to 714 nm is shown in Fig. 3. The measurements are presented in two graphs for clarity.

Common to all curves in the interval 227–377 nm [Fig. 3(a)] is an initial sharp peak originating from two-photon absorption in water.²² Hence, we take the position and width of this peak to mark the point of zero delay and the experimental temporal resolution (0.5 ps), respectively. The two-photon ionization of water produces hydrated electrons, e_{aq}^- , and OH and H radicals. As all the absorption transients across the entire spectrum from 227 to 714 nm are measured on the same absolute scale, the absorption transients around 700 nm resulting from the hydrated electron set an upper limit on contributions from the photoproducts arising from two-photon ionization of water. Accordingly, the absorption pertaining to ionization of water does at most contribute by 1.5 mOD from 227 to 377 nm in good agreement with absorption measurements performed at selected wavelengths when the ICN solution is replaced by neat water. The transient absorption data presented in the subsequent figures have been corrected for the absorption of OH, H, and e_{aq}^- .

The absorption transients from 250 to 377 nm attain their maximum within 0.5 ps and decay by 2/3 to a nearly constant level during the first 20 ps. The spectral profile re-

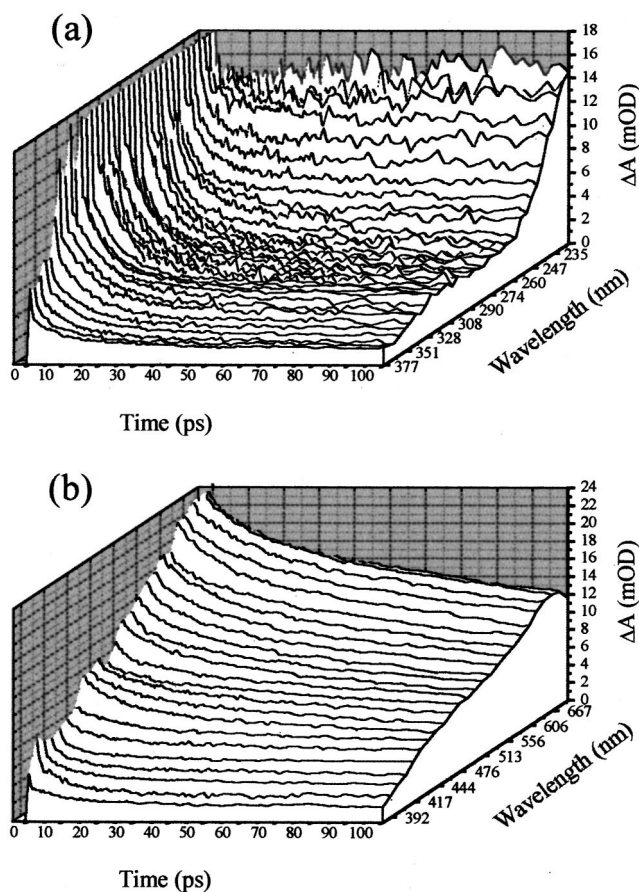


FIG. 3. Pseudo-three-dimensional plot of the induced absorption, $\Delta A(\lambda, t)$, produced when the 266 nm pump pulse photodissociates aqueous ICN. The transients are shown in two graphs for clarity. (a) The measurements from 227 to 377 nm; (b) the transients from 385 to 714 nm. The transients pertaining to two-photon absorption in water have been truncated at 18 mOD.

mains constant at all delays and is well approximated by the absorption spectra of $I(^2P_{3/2})$ and $I(^2P_{1/2})$ assuming a 0.45:0.55 ratio between the total absorption of the two fine-structure components. Hence, we ascribe the absorption transients to atomic iodine and note that *both* dissociation channels are populated in aqueous solution. The iodine atoms are thus observed <0.5 ps after photoexcitation of ICN and the slow decay in the iodine concentration indicates diffusive recombination with the CN fragments. The similarity of the transient absorption dynamics pertaining to $I(^2P_{3/2})$ and $I(^2P_{1/2})$ seems surprising considering that only the $I(^2P_{3/2}) + CN(^2\Sigma^+)$ channel correlates with the $ICN(^1\Sigma^+)$ ground state. However, studies of the photolysis of, for instance, $CS_2(aq)$ show that the solvent-solute interaction greatly enhances nonadiabatic transitions and facilitates recombination processes that otherwise would be forbidden.²³

The strong induced absorption covering the range from 227 to 240 nm rises to its final value in 1 ps. The spectra of the possible photoproducts presented in Fig. 2 peak at significantly longer wavelengths and cannot readily account for the absorption transients. However, guided by the 0.63 eV (28 nm) solvent induced blueshift observed for aqueous ICN and the vicinity of the strong INC absorption spectrum measured in noble gas matrices, we ascribe this spectral feature to aqueous INC. Accordingly, INC is produced in <1 ps and

the concentration of INC molecules changes by less than $\pm 10\%$ during the next 100 ps. The fast formation of the INC molecules indicates that INC is produced by photoisomerization of ICN within the solvent cage, but the peak pertaining to two-photon absorption in water obscures the photodynamics of the first 0.5 ps making it impossible to monitor the transition state dynamics.

The spectral range from 385 to 714 nm is dominated by strong absorption peaking at 667 nm with a spectral shape and temporal development somewhat resembling that reported for hydrated electrons produced by two-photon absorption at 266 nm.²² However, measurements obtained when substituting neat water for the aqueous ICN solution without changing the alignment of the setup displayed a narrower transient absorption spectrum of the hydrated electron with a slightly faster decay than that observed for the ICN solution. The difference between the two data sets clearly reveals the presence of an additional species appearing as the broad shoulder around 450 nm in Fig. 3(b). The absorption of this species decays to roughly 45% of its initial value after 100 ps, but the nonlinear pump intensity dependence of the absorption pertaining to the hydrated electron prevents the accurate determination of its spectrum and temporal development. The spectral characteristics of the shoulder are in good accord with those predicted in Sec. II for the CN radical in water, whereas none of the other products expected from the photolysis of ICN absorb in this spectral region. Hence, we ascribe the 450 nm hump to CN and note that the decay in the $CN(aq)$ absorption transients follows, within the uncertainty of its determination, the dynamics of the aqueous iodine absorption confirming the notion that the iodine and cyanide concentrations decay due to diffusive recombination.

B. Quantum yields

The induced absorption pertaining to INC completely masks the photoinduced depletion of ground state ICN, rendering a direct determination of the quantum yields for I and CN formation and recombination to INC and ICN difficult. Assuming the transient absorption data represent the equilibrated absorption of the species, the quantum yields for the photochemical processes may instead be estimated from the measured induced absorption, ΔA , following the approach described by Thomsen *et al.*²⁴ Accordingly, the quantum yield of a species, X , can be expressed as

$$\Phi(X, t) = \frac{\Delta A(\lambda, t)}{\log(A_{\text{no pump}}) - \log(A_{\text{pump}})}, \quad (1)$$

where the absorption of the probe pulse with overlapping pump pulse, A_{pump} , and without pump pulse, $A_{\text{no pump}}$, is determined from the pump pulse intensity, the length of the sample cell, and the extinction coefficients of the involved species.

Thus, the quantum yield of iodine atoms [$I(^2P_{3/2})$ and $I(^2P_{1/2})$] after 1 ps determined from the absorption transients at 294 nm, $\Delta A(294 \text{ nm}, 1 \text{ ps}) = 12.1 \text{ mOD}$, is $\Phi(I, 1 \text{ ps}) = 38\%$, while subsequent recombination reduces the quantum yield for iodine atoms surviving the first 100 ps [$\Delta A(294 \text{ nm}, 100 \text{ ps}) = 3.1 \text{ mOD}$] to $\Phi(I, 100 \text{ ps}) = 10\%$. Pro-

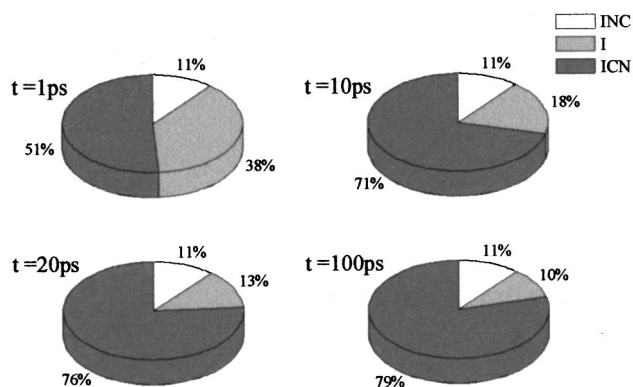


FIG. 4. Graphic representation of the measured quantum yields of ICN, INC, and iodine after 1, 10, 20, and 100 ps. The values should be taken as approximate estimates only due to the uncertainties pertaining to the extinction coefficients and the pulse intensity. See the text for details.

vided the concentration of electronically excited ICN molecules after 1 ps is insignificant, the quantum yield for geminate recombination to either ICN or INC within 1 ps is thus Φ (cage back, 1 ps)=62%. The quantum yield of INC was determined from the induced absorption at 230 nm, ΔA (230 nm, 1 ps)=12.4 mOD corrected for the minor contributions from ICN and I using the INC(aq) absorption spectrum normalized to the maximum extinction coefficient of INC(Ar) ($3739 \text{ M}^{-1} \text{ cm}^{-1}$). The resulting yield is $\Phi(\text{INC}, 1 \text{ ps})=11\%$ leaving $\Phi(\text{ICN}, 1 \text{ ps})=51\%$ for the production of ground state ICN within the first picosecond. As some of the quantities entering the calculations are vitiated with significant uncertainties the relative uncertainty of the above-listed quantum yields is estimated to $\pm 25\%$. The quantum yields are summarized graphically in Fig. 4.

Hence, we conclude that geminate recombination within the solvent cage during the first picosecond is about five times more likely to produce ICN than INC. We also note that the decay in the iodine concentration caused by diffusive recombination with CN molecules outside the cage occurs on a 8 ps time scale and thus significantly slower than the formation of the INC molecules. Now, the extinction coefficient of INC is much larger than that of I potentially leading to a strong increase in the 230 nm absorption transient if even a small fraction of iodine atoms were to slowly recombine with CN and form INC. This is not observed and we therefore conclude that the formation of INC occurs inside the water cage within 1 ps with less than 10% of the INC molecules produced by subsequent diffusive recombination. Hence, iodine atoms that have not recombined with CN to form INC or ICN within the solvent cage and therefore still exist as free species after 1 ps, diffusively recombine with CN outside the cage to form ground state ICN on a 8 ps time scale. The resulting total recombination yield for producing ICN after 100 ps is thus $\Phi(\text{ICN}, 100 \text{ ps})=79\%$.

V. DISCUSSION

The very different recombination behavior of ICN and INC indicates the presence of a barrier for the diffusive reformation of INC. Since *ab initio* gas-phase calculations indicate that the radical reaction $\text{I} + \text{CN} \rightarrow \text{INC}$ is barrierless,¹¹

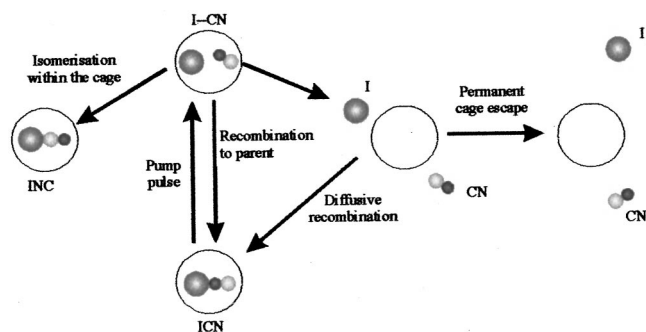


FIG. 5. Model of the photolysis of ICN(aq) when excited at 266 nm. See the text for details.

the lack of diffusive reformation of INC is likely a consequence of solvation. After dissociation and ejection of CN from the water cage the CN fragment thermalizes and becomes hydrated. Due to the higher electronegativity of N, the water molecules principally form hydrogen bonds with the nitrogen end of the CN radical leaving the C atom more accessible to reactions with passing iodine atoms. Hence, ICN is produced by diffusive recombination, while INC is not. Geminate recombination inside the cage, on the other hand, is distinctly different: As shown by Benjamin's MD simulations, ICN and INC may be formed during the first encounter of the recoiling I and CN fragments or result from interconversions during the initial stages of vibrational relaxation on the electronic ground state following recombination. In either case, both isomers are produced and the preferred geminate reformation of ICN likely reflects the fact that ICN is the more stable of the two isomers.

A. Modeling the photolysis

In accordance with the assignments made in Sec. IV A, we have simulated the absorption transients induced by a 150 fs (FWHM) excitation pulse using a first-order rate equation description on the reaction scheme depicted in Fig. 5. Here I-CN is the ICN molecule excited to one of its dissociative states, CN is the ground state CN radical, I represents $\text{I}(^2P_{3/2})$ as well as $\text{I}(^2P_{1/2})$, and INC denotes the ground state INC isomer. The nonexponential behavior of the diffusive recombination process between I and CN is for simplicity simulated by assuming *ad hoc* that part of the CN and I fragments separate permanently. While the diffusive recombination process is more correctly described by, for instance, the Smoluchowski equation, the time-dependent concentrations of I, CN, and ICN governed by diffusive recombination are well approximated by the exponential evolution resulting from the rate equation description.

The induced absorption transients from 227 to 377 nm resulting from the simulations are compared to their experimental counterparts in Figs. 6 and 7(a), while the rate constants resulting from the fit are compiled in Table I. A very satisfactory fit to the measured evolution of all 36 transients is obtained confirming the consistency of the reaction scheme with the available data and the static absorption spectra. The lack of a CN absorption spectrum prevents the extension of the simulations to longer wavelengths. The simulations have utilized the absorption spectra of ICN,

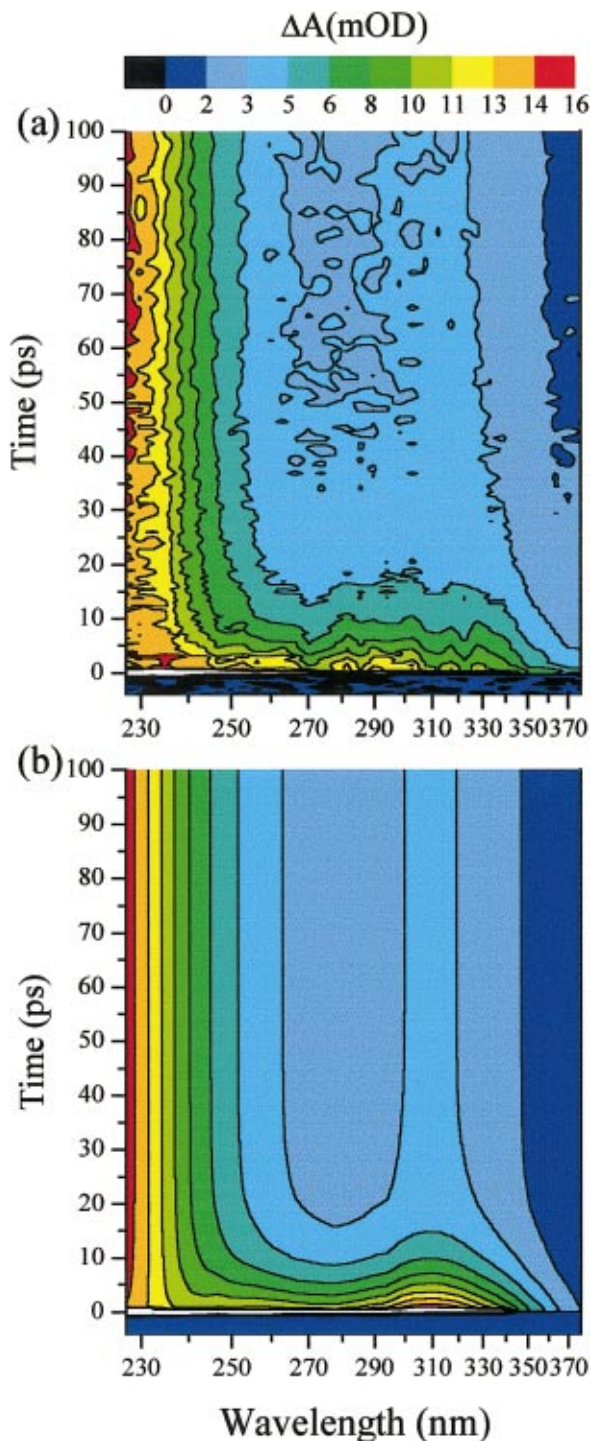


FIG. 6. (Color) Contour plot of (a) the measured transient absorption from 227 to 377 nm and (b) the transient absorption fit based on the model depicted in Fig. 5. The INC isomer is clearly observed as the nearly constant strong absorption at the shortest wavelengths while the two iodine channels give rise to the absorption centered at 308 nm.

$I(^2P_{3/2})$, and $I(^2P_{1/2})$ depicted in Fig. 2 with the 0.45:0.55 ratio between the extinction coefficient \times concentration product for the two iodine fine-structure components determined in Sec. IV A. The maximum extinction coefficient of INC is fixed at $3739 \text{ M}^{-1} \text{ cm}^{-1}$, while the wavelength of maximum absorption and spectral width have been adjusted to give the best overall agreement with the absorption transients in the

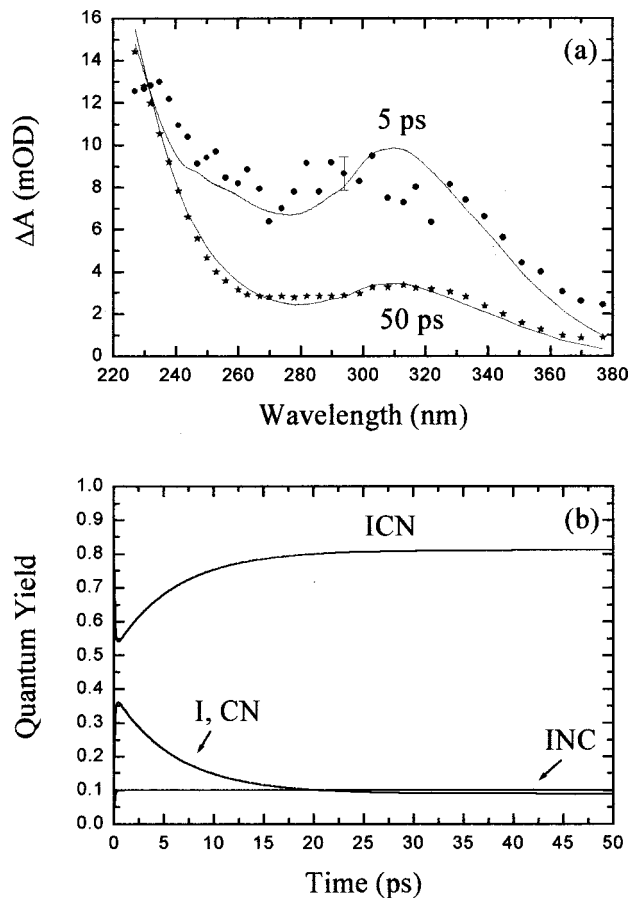


FIG. 7. (a) Relative concentrations of ICN, I, CN, and INC as a function of time derived from the simulation of the absorption transients. (b) Comparison of the measured and the fitted (curves) transient absorption spectra 5 and 50 ps after the photodissociation pump pulse.

range from 227 to 250 nm. The resulting INC spectrum peaks at $212 \pm 5 \text{ nm}$ with a width of $40 \pm 5 \text{ nm}$ (FWHM). The blueshift of approximately 38 nm is similar to the blueshift of ICN(aq) and the width is only a few nanometers wider than that of INC in solid argon and krypton.¹¹

The concentration dynamics of ICN, I, CN, and INC shown in Fig. 7(b) reveal that more than half of the ICN molecules are reformed during the pump pulse and the rest are produced by recombination on an 8 ps ($1/e$) time scale. Geminate recombination forming INC occurs in 1 ps and the good agreement with the experimental data is obtained assuming no additional contributions to the INC concentration. In particular, the transient absorption spectra show no sign of HCN resulting from hydrogen abstraction nor does it reveal

TABLE I. Rate constants used with the model presented in Fig. 5 to simulate the transient absorptions.

Reaction	Rate constant (ps^{-1})
Dissociation	3.8
Geminate reformation of ICN	5.2
Geminate isomerization	1.0
Diffusive reformation of ICN	0.125
Permanent cage escape	0.038

the presence of any vibrationally excited species. The vibrational relaxation of ICN and INC formed by geminate recombination is addressed in the Sec. V B.

B. Vibrational relaxation of INC and ICN

Geminate recombination through nonadiabatic transfer to the electronic ground state leaves the molecules in highly excited vibrational states close to the dissociation limit. In the triatomic molecules $\text{ClO}_2(\text{aq})$ and $\text{CS}_2(\text{aq})$ the absorption spectra of the vibrationally excited species are more than three times as wide as that of the vibrational ground state resulting in wide transient absorption spectra during the first 10 ps after recombination. These spectra narrow and approach that of the vibrational ground state as the molecules relax. In contrast, the good agreement between the ICN(aq) photolysis experiment and model is obtained using equilibrated INC and ICN absorption spectra at all times. This indicates that INC and likely also ICN (although its absorption is barely detectable) have only little vibrational energy after 1 ps, implying that most of the ~ 3 eV excitation energy remaining after recombination is dissipated to the solvent on a subpicosecond time scale.

To further investigate the vibrational relaxation process of INC(aq) we have calculated the relaxation time using both the semiclassical golden rule formalism and classical molecular dynamics simulations. The two calculations show that subpicosecond vibrational relaxation is possible only if it occurs in the bending or IN stretching modes.

The two theoretical treatments are now discussed in detail beginning with the golden rule approach described by, for instance, Poulsen *et al.*²⁵ According to this description the transition rate k_{ij} between two adjacent levels, i and j , can be expressed as

$$k_{ij} = \frac{2\hbar^{-2}}{1 + \exp(-\hbar\omega_{ij}/k_B T)} \sum_{\alpha, \beta=1}^3 \langle i|q_\alpha|j \rangle \times \langle j|q_\beta|i \rangle \int_{-\infty}^{\infty} dt \exp(i\omega_{ij}t) \langle F_\alpha(t)F_\beta(0) \rangle, \quad (2)$$

where $\omega_{ij} = E_i - E_j$ is the energy spacing between the two vibrational levels, q_α and q_β are dimensionless normal coordinates, and F_α is the classical bath force along normal mode α . Accordingly, the relaxation time $\tau_{ij} = 1/k_{ij}$ is inversely proportional to both the vibrational coupling elements and the classical bath force autocorrelation spectrum evaluated at the vibrational energy gap. Force autocorrelation functions calculated for the relevant normal modes in the aqueous systems of H_2O in H_2O ,²⁶ N_3^- in water,²⁷ CN^- in water,²⁸ and ClO_2 in water²⁵ differ by less than an order of magnitude. Hence, the force spectrum depends only moderately on the solute and is for the present estimate of vibrational relaxation of aqueous INC approximated by that of ClO_2 in water calculated by Poulsen *et al.*²⁵ and depicted in Fig. 8. Adjusting expression (2) for quantum mechanical corrections²⁵ leads to a 14 ps vibrational relaxation time ($1/e$) of the first excited asymmetric stretch mode ($\nu_3 = 1130 \text{ cm}^{-1}$) of $\text{OCIO}(\text{aq})$ in good agreement with the 10 ps ($1/e$) relaxation time observed experimentally.²⁹

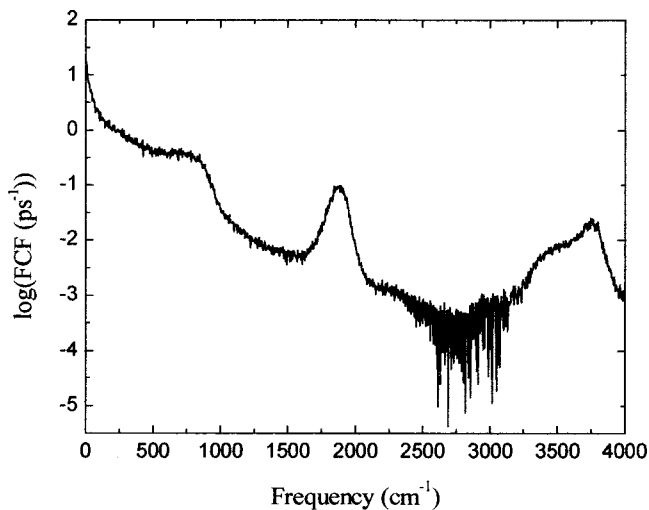


FIG. 8. Force autocorrelation function of ClO_2 in water (Ref. 25).

The fundamental vibration frequencies of INC calculated by Samuni *et al.*⁸ are 479.2 cm^{-1} (IN stretch), 247 cm^{-1} (bend), and 2026.5 cm^{-1} (CN stretch). The relatively low vibrational frequencies of the IN stretch and INC bending modes result in force correlation function amplitudes, which are nearly two orders of magnitude higher than that of the fundamental asymmetric stretch of $\text{OCIO}(\text{aq})$, while the amplitude of the force autocorrelation function associated with the high frequency CN stretch is an order of magnitude lower (see Fig. 8). Owing to the harmonic ground state potential at low energies, the dominating coupling matrix elements of the rate limiting transitions between the lowest vibrational states of INC are approximately equal to the harmonic coupling elements of $\text{OCIO}(\text{aq})$. Consequently, if the vibrational relaxation predominantly proceeds via the bending or IN stretch modes, the relaxation time of INC(aq) is expected to be of the order of 0.1–1 ps in accord with the fast relaxation observed experimentally. If, on the other hand, the rate limiting vibrational transitions close to the bottom of the ground state potential involves the CN stretch we estimate a relaxation time in excess of 10 ps. The vibrational frequencies of ICN are 486 cm^{-1} (C–I stretch), 305 cm^{-1} (bend), and 2188 cm^{-1} (CN stretch)⁸ and the same arguments therefore also suggest that vibrationally excited ICN(aq) relax to the vibration ground state on a subpicosecond time scale.

The MD simulations of the vibrational relaxation employ a fixed number, volume, and energy (*NVE*) ensemble of one INC molecule and 511 flexible SPC H_2O molecules³⁰ in a cube with a side length of 24.86 \AA corresponding to a density of 0.997 g/cm^3 . The INC geometry is optimized by a DFT/B3LYP calculation using the LANL2DZ basis set while the intramolecular force field of INC is derived from electronic structure calculations utilizing the GAUSSIAN 98 program package.³¹ The resulting bond lengths and frequencies, listed in Table II, compare favorably to theoretical values obtained by Samuni *et al.*⁸ as well as experimental values measured in argon matrices. A normal mode analysis based on GAUSSIAN 98 calculations leads to the following approximate valence bond intramolecular potential:

TABLE II. Spectroscopic properties of INC.

Spectroscopic property	This work	Samuni <i>et al.</i> (Ref. 8)	Argon matrix (expt) (Ref. 8)
r_{IN} (Å)	2.004	1.991	
r_{CN} (Å)	1.203	1.203	
μ (D)	3.57	3.50	
ω_{bend} (cm^{-1})	273	227	≈ 200
ω_{IN} (cm^{-1})	459	479	494
ω_{CN} (cm^{-1})	2073	2073	2057.5
k_{CN} (hartree/bohr ²)	0.992		
k_{NI} (hartree/bohr ²)	0.182		
k_{θ} (hartree/rad ²)	0.0135		

$$V_{\text{INC}} = \frac{1}{2}k_{\text{CN}}(r_{\text{CN}} - r_{\text{CN}}^{\text{eq}})^2 + \frac{1}{2}k_{\text{IN}}(r_{\text{IN}} - r_{\text{IN}}^{\text{eq}})^2 + \frac{1}{2}k_{\theta}(\theta - \pi)^2 \quad (3)$$

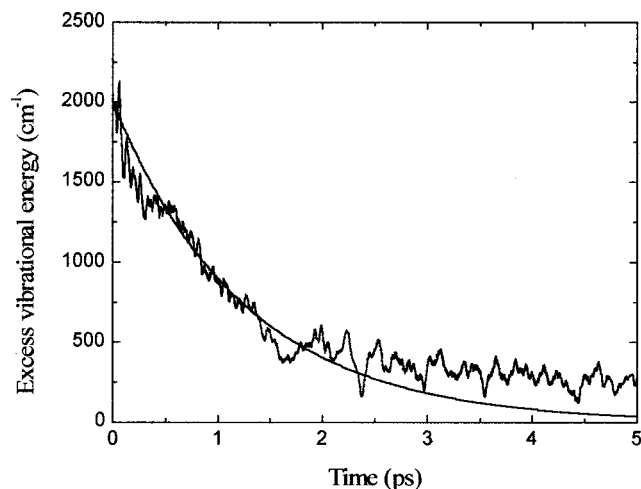
with the force constants listed in Table II. Consistent with Eq. (3), r_{CN} and r_{IN} become actual vibrational modes of the molecule.³² The electrostatic charges on I ($q=0.16e$), C ($q=-0.27e$), and N ($q=0.11e$) are calculated from the Merz–Kollman scheme, while the van der Waals interactions between solute and solvent are described by Lennard-Jones interactions between any atom in INC and H₂O. The particular ϵ and σ parameters of the H₂O–INC Lennard-Jones potential are derived by applying standard Lorentz-Berthelot–mixing rules to single atom–atom ϵ and σ values obtained from Refs. 33 and 34 and listed in Table III.

The system is propagated in steps of 0.5 fs using the Verlet algorithm³³ and standard periodic boundary conditions with half box-length spherical cutoff. First, the initial 20 geometries used in the simulations are extracted from a 20 ps trajectory run equilibrated at 300 K by sampling one system configuration for every picosecond. The INC molecule is then excited by deforming the bond in question and propagated for 5 ps, while monitoring the total energy of the INC molecule. Initial excitation energy of 10 kT is chosen in order to follow the rate limiting transitions close to the bottom of the potential while keeping the potential energy within the valence bond approximation.

Figure 9 shows the excess vibrational energy relaxation of INC when a potential energy of $10k_B T = 2080 \text{ cm}^{-1}$ is stored in the IN bond. The energy relaxation decays exponentially with a time constant of 1.2 ps ($1/e$) leaving an excess vibration energy of only $\approx 250 \text{ cm}^{-1}$ after 3 ps. Hence, the fast relaxation of the IN stretch is in good agreement with the result of the golden rule estimate. The corresponding results for the CN bond dynamics showed no sign

TABLE III. Lennard-Jones parameters describing the interaction between INC and H₂O.

Atom pair	σ (Å)	ϵ/k_B (K)
I–H	3.31	45.5
I–O	3.38	121.4
C–H	3.08	20.9
C–O	3.15	55.9
N–H	3.06	17.9
N–O	3.13	49.9

FIG. 9. Simulated vibrational energy relaxation of the IN stretch excited by 2080 cm^{-1} . The vibrational excitation energy decays in 1.2 ps ($1/e$).

of energy relaxation within the first 5 ps likewise supporting the golden rule estimate. Vibrational relaxation in the bending mode was not investigated, but from the force correlation amplitude depicted in Fig. 8 it is expected to be even faster than relaxation in the IN stretch. In accordance with the conclusions based on the golden rule estimates, the MD simulations thus lead us to infer that the CN stretch is not significantly involved in the vibrational relaxation of INC.

C. Comparison with MD simulations of ICN in chloroform

The detailed experimental information about the ICN(aq) photodynamics now enables the comparison with the MD simulations performed by Benjamin.¹⁰ However, due to the strong blueshift of the ICN(aq) absorption spectrum relative to that in chloroform and the fact that hydrogen bonded water constitutes a stronger solvent cage than chloroform, perfect agreement with theory is not to be expected. Nevertheless, the estimated 62% quantum efficiency for geminate recombination of ICN in water compares favorably with the simulations and the $\approx 5:1$ ratio between the quantum yield of ICN and INC measured in aqueous solution is also in fair agreement with the simulated recombination yields.¹⁰ The reaction dynamics are faster in water, though. According to the MD simulations the vibrationally excited molecule formed by geminate recombination performs several interconversions between the ICN and INC configurations before energy dissipation to the solvent freezes the molecule in its metastable or stable geometry after ≈ 3 ps. This is slower than the 1 ps upper limit for the isomerization measured in aqueous solution suggesting a more efficient energy dissipation to water.

MD simulations of the geminate recombination of ICN in chloroform show that the CN stretch becomes excited by $\approx 2100 \text{ cm}^{-1}$ when ICN is formed on the electronic ground state. The CN vibration persists for more than 5 ps after geminate recombination and Benjamin infers that the vibrational relaxation predominantly occurs in the bending and

CN stretch modes. The long CN stretch relaxation time determined by Benjamin agrees with the calculated relaxation time of the CN stretch of INC presented previously, but the subpicosecond relaxation time observed experimentally suggests that the CN stretch is not significantly involved in the relaxation process. Further experimental as well as theoretical studies are obviously needed to uncover the finer details of the vibrational relaxation of ICN and INC.

VI. CONCLUSION

In summary, our study of the photolysis of aqueous ICN at 266 nm shows that caging of the I and CN photoproducts by the surrounding water molecules limits the I and CN quantum yield to 38% after 1 ps. Diffusive recombinations involving I and CN fragments that do escape the solvent cage further reduces the yield to 10% during the subsequent 100 ps. Diffusive recombination produces only ICN—not INC. This product distribution is explained in terms of the higher electronegativity of N than of C. Thus hydrogen bonding between CN and H₂O will involve complexes like CN···H–OH, which polarize the orientation of CN and facilitate the reaction leading to ICN.

The majority of the dissociating ICN molecules retained within the solvent cage recombine to form ICN in ≈ 1 ps, while a minor fraction isomerizes to INC. ICN and INC relax to the vibrational ground state in ≈ 1 ps in good agreement with theoretical estimates based on the golden rule formalism and MD simulations assuming the vibrational relaxation proceeds via the IC/IN stretch and ICN/INC bending modes. However, the details of the cage back reaction and the subsequent vibrational relaxation process are not experimentally observable with the present time resolution. Hence, the fundamental question of to what extent isomerization of ICN in solution is due to rotational reorientation of the dissociating fragments prior to recombination and to interconversion during the vibrational relaxation is still unsettled and remains open to further investigation.

ACKNOWLEDGMENT

The many fruitful discussions with Svend Knak Jensen are highly appreciated.

- ¹J. Thøgersen, C. L. Thomsen, J. A. Poulsen, and S. R. Keiding, *J. Phys. Chem. A* **102**, 4186 (1998).
- ²C. L. Thomsen, J. Thøgersen, and S. Keiding, *J. Chem. Phys.* **114**, 4099 (2001).
- ³C. L. Thomsen, P. J. Reid, and S. R. Keiding, *J. Am. Chem. Soc.* **122**, 12795 (2000).
- ⁴S. Hess, H. Bürsing, and P. Vöhringer, *J. Chem. Phys.* **111**, 5461 (1999).
- ⁵P. K. Walhout, C. Silva, and P. F. Barbara, *J. Phys. Chem.* **100**, 5188 (1996).
- ⁶T. Kühne and P. Vöhringer, *J. Chem. Phys.* **105**, 10788 (1996).
- ⁷D. D. Davis and H. Okabe, *J. Chem. Phys.* **49**, 5526 (1968).
- ⁸U. Samuni, S. Kahana, R. Fraenkel, Y. Haas, D. Danovich, and S. Shaik, *Chem. Phys. Lett.* **225**, 391 (1994).
- ⁹W. P. Hess and S. R. Leone, *J. Chem. Phys.* **86**, 3773 (1987).
- ¹⁰I. Benjamin, *J. Chem. Phys.* **103**, 2459 (1995).
- ¹¹J. Helbing, M. Chergui, S. Fernandez-Alberti, J. Echave, N. Halberstadt, and J. A. Beswick, *Phys. Chem. Chem. Phys.* **2**, 4131 (2000).
- ¹²C. Wan, M. Gupta, and A. H. Zewail, *Chem. Phys. Lett.* **256**, 279 (1996).
- ¹³I. Benjamin and R. Wilson, *J. Chem. Phys.* **90**, 4176 (1989).
- ¹⁴A. I. Krylov and R. B. Gerner, *J. Chem. Phys.* **100**, 4242 (1994).
- ¹⁵E. A. Coronado, V. S. Batista, and W. H. Miller, *J. Chem. Phys.* **112**, 5566 (2000).
- ¹⁶W. M. Pitts and A. P. Baronavski, *Chem. Phys. Lett.* **71**, 395 (1980).
- ¹⁷A. Treinin and E. Hayon, *J. Am. Chem. Soc.* **97**, 1716 (1975).
- ¹⁸P. Fournier de Violet, R. Bonneau, and J. Jousot-Dubien, *Chem. Phys. Lett.* **19**, 251 (1973).
- ¹⁹The spectrum of iodine is reported by Fournier de Violet and the extinction coefficient is reported by Treinin *et al.* The basis for the extinction coefficient measurement is not known.
- ²⁰R. Foster, *Molecular Association* (Academic, London, 1979).
- ²¹A. Thoma, G. Schalmoser, A. M. Smidt, B. E. Wurfel, and V. E. Bondybey, *J. Chem. Phys.* **100**, 5387 (1994).
- ²²C. L. Thomsen, D. Madsen, S. R. Keiding, J. Thøgersen, and O. Christiansen, *J. Chem. Phys.* **110**, 3453 (1999).
- ²³C. L. Thomsen, D. Madsen, J. Thøgersen, J. R. Byberg, and S. R. Keiding, *J. Chem. Phys.* **111**, 703 (1999).
- ²⁴C. L. Thomsen, D. Madsen, J. A. Poulsen, C. Rønne, J. Thøgersen, S. J. K. Jensen, and S. R. Keiding, *J. Chem. Phys.* (to be published).
- ²⁵J. Poulsen, T. M. Nymand, and S. R. Keiding, *Chem. Phys. Lett.* **343**, 581 (2001).
- ²⁶J. A. Poulsen (private communication).
- ²⁷A. Morita and S. Kato, *J. Chem. Phys.* **109**, 5511 (1998).
- ²⁸R. Rey and J. T. Hynes, *J. Chem. Phys.* **108**, 142 (1998).
- ²⁹J. A. Poulsen, C. L. Thomsen, S. R. Keiding, and J. Thøgersen, *J. Chem. Phys.* **108**, 8461 (1998).
- ³⁰K. Toukan and A. Rahman, *Phys. Rev. B* **31**, 2643 (1985).
- ³¹M. J. Frisch, W. Trucks, H. B. Schlegel *et al.*, GAUSSIAN 98, Pittsburgh (1998).
- ³²By adopting this particular form of the potential a mixed term of the type $k_{\text{CN,IN}}(r_{\text{CN}} - r_{\text{CN}}^{\text{eq}})(r_{\text{IN}} - r_{\text{IN}}^{\text{eq}})$ has been neglected. However, this term is small, $k_{\text{CN,IN}} = -0.97 \text{ eV/\AA}^2$.
- ³³M. P. Allen and D. J. Tildesley, *Computer Simulations of Liquids* (Oxford University Press, Oxford, 1987).
- ³⁴S. F. Alberti, J. Echave, V. Engel, N. Halberstadt, and J. A. Beswick, *J. Chem. Phys.* **113**, 1027 (2000).
- ³⁵J. U. White, *J. Chem. Phys.* **8**, 79 (1940).